Research article

Determination of dielectric properties of lead-contaminated soils: Potential application to soil remediation

Samroeng Santalunai [a], Jariya Pakprom [a], Weerawat Charoensiri [a],
Chanchai Thongsopa [a], Thanaset Thosdeekoraphat [a], Pisit Janpangngern [a],
Teerapon Yodrot [b], Nuchanart Santalunai [c,*], Samran Santalunai [a,*]

[a] School of Electronic Engineering, Institute of Engineering, Suranaree University of Technology, 30000, Nakhon Ratchasima, Thailand
[b] Department of Electrical Engineering Technology, Faculty of Industry and Technology, Rajamangala University of Technology Rattanakosin, wang klai kangwon campus, 77110, Prachuap Khiri Khan, Thailand
[c] Department of Telecommunication Engineering, Faculty of Engineering and Technology, Rajamangala University of Technology Isan, 30000, Nakhon Ratchasima, Thailand

ARTICLE INFO

ABSTRACT

This research investigated the effectiveness of radio frequency (RF) heating as a treatment for lead-contaminated soil, assessing its impact through dielectric constant measurements. Using water-soluble lead (II) acetate trihydrate, the study analyzed the impact of RF heating on soil dielectric properties under various soil moisture conditions (high, medium, and low) and electric field strengths (112.5, 150, 225, and 450 kV/m). The results indicated that soil temperature increased with lead concentration, highlighting significant changes in soil thermodynamics. Under high-humidity conditions, temperature increases were more pronounced, suggesting that higher lead concentrations elevate soil temperatures. Moreover, RF heating consistently reduced the dielectric constant as lead concentration increased, which was especially evident at higher electric field strengths. The study found that the soil resistivity approached that of uncontaminated soil, particularly at 450 kV/m electric field strength, with the highest removal rate of 46.154%. This investigation provides valuable insights into the application of RF heating for soil quality improvement in lead-contaminated environments, demonstrating how dielectric properties can reflect those of uncontaminated soil.

1. Introduction

Lead contamination has become a significant issue, affecting soil quality and causing adverse effects on both the environment and human health [1]. The increasing global population and industrial growth exert pressure on agricultural land demand [2][3][4][5][6][7]. Human activities, a major contributor to agricultural soil contamination [8][9], pose significant threats to aquatic and terrestrial life. Lead is durable and highly toxic, with relatively low electrical conductivity compared with other metals. It contains non-essential elements that can impact plant metabolic processes, affecting growth and development, leading to poor root growth, abnormalities, oxidative stress, reduced biomass production, inhibited germination, and compromised photosynthesis

---

* Corresponding authors.
E-mail addresses: nuchanart.fa@rmuti.ac.th (N. Santalunai), samran.sa@sut.ac.th (S. Santalunai).

Table 1
Comparison of different soil remediation methods.

Method	Advantages	Disadvantages	Types of Contaminants	Efficacy
Physical (Soil Replacement, Hydrothermal)	Enhances soil environmental capacity	High cost, long absorption times	Heavy metals, organics	Variable
Chemical (Chelates, Organic Acids, Biomaterials)	Effective for various metals	Potential chemical hazards	Pb, Cu, Zn	High
Electrokinetic Rehabilitation	Ease of installation, low cost	Requires electrical setup	Pb, other heavy metals	Moderate to high
Bioremediation (Phytoremediation, **Microbial**)	Ecologically safe, sustainable	Slow, affected by environmental factors	Heavy metals, organics	Moderate
RF Heating (based on dielectric heating)	Rapid, uniform heating, minimum soil structure disturbance, works on dry and wet soils, faster treatment	Energy consumption, equipment cost	Pb, other heavy metals	High

[10][11][12][13][14][15]. Consequently, the presence of lead ions in soil poses a risk to natural ecosystems and is a global issue because lead is widely used in agriculture and domestic activities [16][17].

Efforts to address lead contamination in natural resources have intensified globally, with researchers using various remediation methods, including physical, chemical, and biological techniques [18]. Physical remediation, such as soil replacement and hydrothermal treatment, cleans soil but is costly and time consuming. Chemical remediation includes several techniques such as restoration, fixation, electrokinetic rehabilitation, and vitrification, which utilize chelates, organic acids, and biomaterials [19]. Chemical soil washing separates heavy metals such as lead, copper, and zinc [20][21][22], while immobilizing them to reduce migration [23][24][25][26]. Electrokinetic rehabilitation applies electrical voltage to move lead particles to electrodes, effectively removing heavy metals [27][28]. Vitrification heats soil to high temperatures to remove contaminants but is energy intensive and costly [29].

Bioremediation, categorized into phytoremediation and microbial bioremediation, uses plants and microorganisms to absorb or neutralize contaminants but can be slow and environmentally limited [30][31][32][33][34][35][36]. Adsorption methods involving materials such as charcoal and nanomaterials are complex and time consuming [37][38][39][40][41][42][43]. Traditional methods, such as ion exchange, electrolysis, chemical precipitation, solvent extraction, and biological techniques, are costly and resource intensive [44].

In contrast, using high-frequency waves for soil remediation offers an efficient solution. This method allows precise control over soil temperature and treatment duration through dielectric heating [45]. Electromagnetic fields have proven effective in various environmental processes [46][47][48][49][50][51][52]. Radio frequency (RF) heating rejuvenates soil through vapor extraction or biodegradation and penetrates deeply, covering larger areas. It works well with various materials, including those with low-moisture content [53]. At frequencies between 10 and 100 MHz, RF heating generates heat within the soil as the electric field component causes polar molecules to oscillate, producing heat through dielectric loss. This results in rapid, uniform heating, which is effective for treating large volumes of contaminated soil. The depth of RF penetration depends on the frequency and soil dielectric properties, allowing targeted heating at various depths, which is beneficial for reaching unevenly distributed contaminants.

RF heating technology based on dielectric heating uses high-voltage alternating current signals with parallel electrodes configured as a capacitor. The medium to be heated is placed between these electrodes, causing polar molecules to align and vibrate with the alternating electric field. Heat is generated through structural loss and friction during molecular interaction. As the frequency increases, more energy is transferred, resulting in more efficient heating; however, there is an upper frequency limit due to molecular structural limits [54][55]. This method provides uniform heating, ensuring that the entire medium is evenly heated, which is beneficial for materials like soil. RF heating can penetrate deeply, making it effective for large volumes of soil, and works well even in low-moisture conditions. The ability to control the heating process precisely by adjusting frequency and intensity enhances efficiency, preventing energy wastage and quickly achieving the desired temperature [56][57].

In the context of soil remediation, RF heating ensures that the energy is evenly distributed throughout the soil, making it particularly useful for large-scale projects. This uniform heating helps in breaking down contaminants and enhances the overall soil quality. Furthermore, RF heating can be integrated with other remediation techniques, such as chemical or biological methods, to improve overall efficiency and effectiveness [58][59]. Overall, RF heating based on dielectric heating is a promising technology for soil remediation. Its ability to provide uniform, deep, and efficient heating makes it ideal for large-scale projects, and its effectiveness in low-moisture conditions adds to its versatility. By ensuring uniform energy distribution and allowing precise control over the heating process, RF heating stands out as an advanced method for improving soil quality and addressing contamination issues.

Table 1 displays a comparison of different soil remediation methods. It summarizes the advantages and disadvantages of various traditional and modern remediation techniques, highlighting the potential of RF heating as a superior alternative owing to its efficiency, control, and versatility in different environmental conditions.

This study investigates the application RF heating based on dielectric heating for treating lead-contaminated soil. The research focuses on two main objectives:

1) To measure and compare the dielectric properties of lead-contaminated soil (using lead (II) acetate trihydrate) with those of uncontaminated soil.

Table 2
Parameters of soil sample preparation.

Parameter	Value
Soil	100 g
Particle size	0.10 – 0.25 mm
Porosity	0.69
Volume of soil jars	100 cm^3
Bulk density	0.85 g/cm^3
Lead Pb (II) acetate 3-hydrate	200, 600, 1000 mg/L

2) To evaluate the impact of RF heating on the reduction of lead contamination in soil through dielectric property measurement and X-ray fluorescence (XRF) analysis of soil subjected to RF heating with paired electrode plates, which is conducted for the first time in this study.

These objectives aim to advance the understanding and application of RF heating technology in soil remediation, ultimately supporting the development of effective and sustainable soil management strategies. The findings from this study are expected to contribute significantly to environmental protection and the advancement of soil remediation technologies.

2. Materials and methods

2.1. Soil sample preparation

The soil sample utilized in the test was obtained from rice fields in Surin Province, situated in the northeastern region of Thailand. The soil was prepared by drying it through sun exposure for 24 h. After drying, the soil underwent thorough blending and sieving to eliminate large particles, resulting in soil particles ranging from 0.10 mm to 0.25 mm, which is the ideal size range for the subsequent experimental phase [60]. The processed soil was then contaminated with lead (II) acetate trihydrate, serving as the surrogate in this experiment. Lead (II) acetate trihydrate is a suitable laboratory surrogate for naturally occurring lead contamination. This compound is commonly used in soil contamination research because it is a highly pure chemical, allowing precise control of lead concentration in experiments. Its high solubility in water ensures good dispersion in soil, closely simulating natural contamination. Additionally, it offers ease of handling and safety in laboratory settings, unlike naturally contaminated soil, which may contain uncontrollable factors or impurities. Previous studies have also employed this compound for similar purposes [61][62].

For the simulated contamination, three concentrations of lead (II) acetate trihydrate were applied: 200, 600, and 1000 mg/L. All processed soil samples were stored in glass dishes (9.3 cm diameter × 1.5 cm height), each containing 100 g of soil. The soils were categorized into two groups: normal soil and soil contaminated with lead at concentrations of 200, 600, and 1000 mg/L. Group 1 was exclusively designated for measuring the dielectric constant, while Group 2 underwent RF wave heating tests before dielectric constant measurements in the subsequent step. This comparative approach aimed to evaluate the dielectric constant of these two groups. The material preparation specifics are detailed in Table 2.

The initial step in soil sample preparation involved producing a dry soil sample specifically designed for testing. This sample was loaded into a 100 g glass dish, where it underwent thorough blending and filtering to eliminate large soil particles [63], resulting in soil grain sizes of 0.10–0.25 mm, which are suitable for testing. Subsequently, water contaminated with lead concentrations of 200, 600, and 1000 mg/L was injected to achieve 69% porosity. After completing this process, the soil was left to dry at high-, medium-, and low-humidity levels. Specifically, the criteria for these three humidity levels in soil were set to simulate different environmental conditions and assess how moisture content affects the dielectric properties and RF heating efficiency in lead-contaminated soil. High humidity ($\approx$ 30% moisture) represents wet conditions, medium humidity ($\approx$ 20% moisture) simulates typical field conditions, and low humidity ($\approx$ 10% moisture) emulates dry conditions. These criteria facilitate the understanding of the soil moisture impact on dielectric properties and RF heating effectiveness. By testing soils with varying humidity levels, the study provides comprehensive and reliable results applicable to real-world scenarios. The soil samples at different humidity states are shown in Fig. 1.

2.2. Experimental design of an RF heating system

The proposed RF heating system has a total power of 9 kW and a frequency of 40.68 MHz, which falls within the common industrial heating range of 10–50 MHz [64]. Additionally, the authorized frequencies for medical, scientific, and industrial applications are 13.56, 27.12, and 40.68 MHz, respectively [65]. This RF heating system consists of two electrode pads, each measuring 520 mm × 520 mm. The top plate serves as the cathode, while the bottom plate acts as the anode. The distance between the top and bottom plates can be adjusted using the top plate, allowing the electric field strength to be modified relative to the distance between the two pads. In contrast, the bottom plate is fixed.

Based on practical factors pertaining to the apparatus and experimental setup, electric field strengths of 112.5, 150, 225, and 450 kV/m were calculated. The field strengths in our RF heating experiments were specifically defined by the plate spacing and voltage drop across the plates of the high-frequency generator. Considering the constraints imposed by the high-frequency generator's plate level, the study team opted to employ plate distances of 2, 4, 6, and 8 cm [66][67]. These values are regular intervals that enable consistent and replicable experiments. By putting precise plate separation lengths into Eq. (1) [68][69] and using a 9 kW voltage drop across the two plates, we calculated the corresponding electric field strengths. Thus, when performing experiments under the
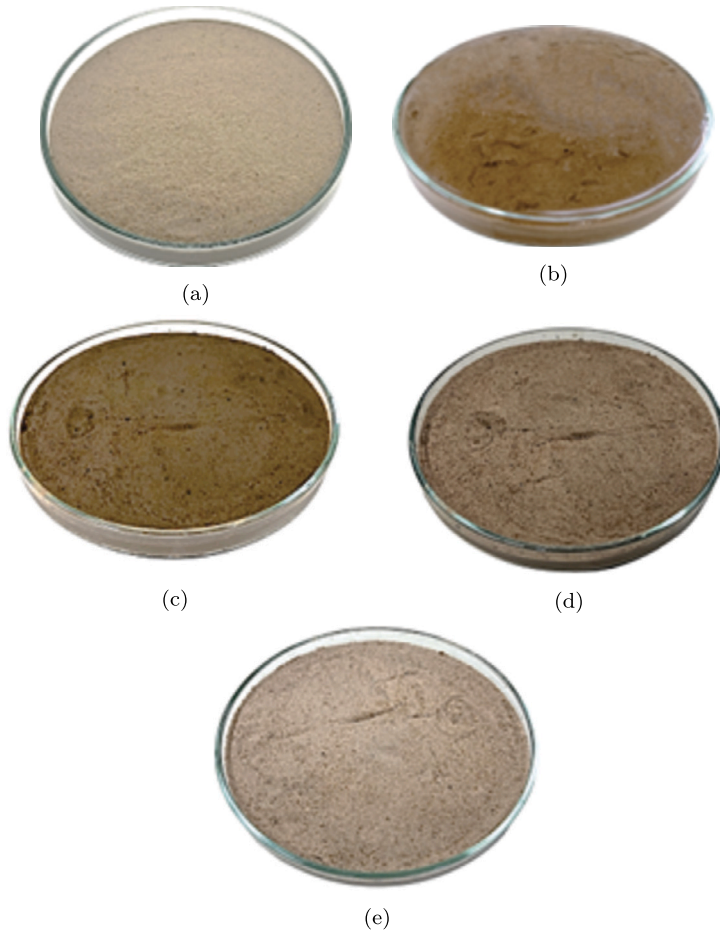
Fig. 1. Soil samples at different humidity states: (a) uncontaminated soil, (b) lead-contaminated soil, (c) high-moisture soil, (d) medium-moisture soil, and (e) low-moisture soil.

aforementioned conditions, the electric field intensities were measured to be 450 kV/m at 2 cm spacing, 225 kV/m at 4 cm, 150 kV/m at 6 cm, and 112.5 kV/m at 8 cm. Previous studies [70][71] had obtained similar results.

$$E = \frac{\sigma}{\varepsilon} = \frac{\upsilon}{\Delta d} \tag{1}$$

where ε is the dielectric constant, υ is the voltage drop between plates, Δd is the distance between plates, and σ is the conductivity of the dielectric material.

The behavior of the dielectric constant in response to waves at various frequencies is described by its complex permittivity. Dielectric materials can convert electrical energy into heat energy. The heat generated is an outcome of the interaction between frequency energy and a medium with dielectric properties characterized by a polar molecular structure. This structure can induce waves that, in turn, transform into heat, as described by Eq. (2) [72].

$$\rho C_{\mathrm{p}} \frac{\Delta T}{\Delta t} = 5.563 \times 10^{-11} f E^2 \varepsilon'' \tag{2}$$

where C_{p} is the specific heat, ρ is the density of the material, E is the electric field intensity, t is the time, ΔT is the temperature increase in the material, f is the frequency.

The proposed configuration enables accurate manipulation of the electric field intensity levels at 112.5, 150, 225, and 450 kV/m to attain the targeted heating rate, with $d_1 = 8$ cm, $d_2 = 6$ cm, $d_3 = 4$ cm, and $d_4 = 2$ cm, as depicted in Fig. 2a. The study also considered the temperature distribution in the system, as illustrated in Fig. 2b, which displays a homogeneous temperature distribution. The objective of this consideration is to achieve ideal outcomes in the most efficient heating procedure. Electric field waves propagate from regions of positive voltage toward the negative terminal on the plate.

The ability to penetrate the frequency spectrum is a critical factor that must be carefully considered for the intended material. This can be determined through wave penetration, which can be calculated using Eq. (3) [73][74] [75].
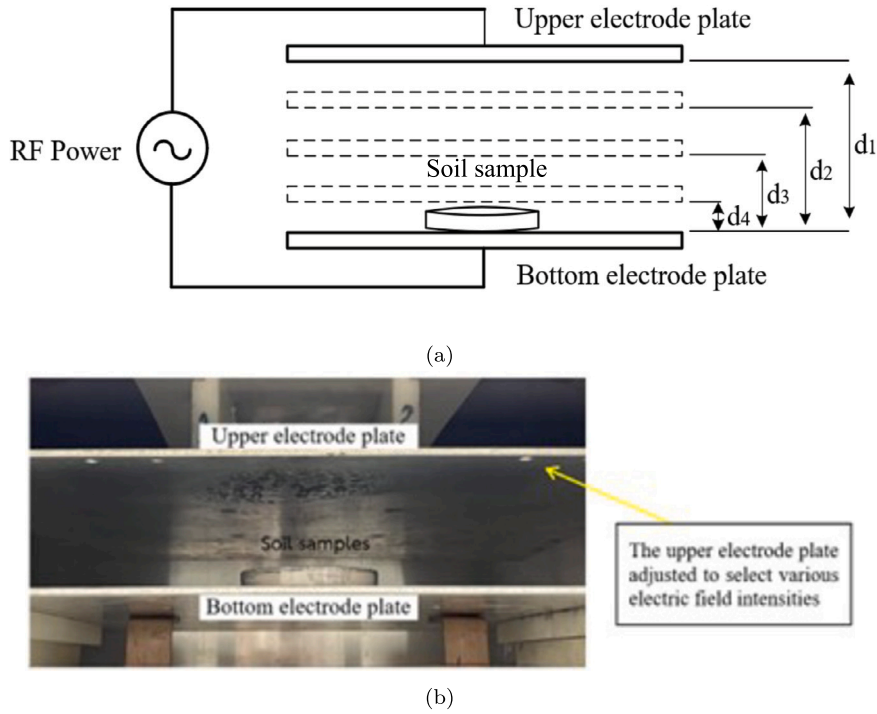
(a)

(b)

Fig. 2. RF heating pattern: (a) RF heating of lead-contaminated soil samples at different distances; (b) RF heating example.
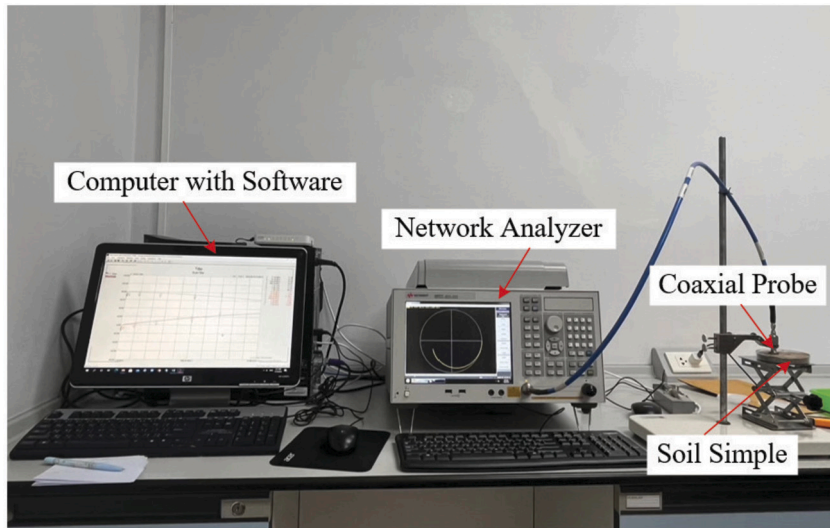

Fig. 3. Experimental configuration for measuring dielectric constant properties.

$$d_{\mathrm{p}} = \frac{c}{2\pi f \sqrt{2\varepsilon'[\sqrt{1 + (\varepsilon''/\varepsilon')^2} - 1]}} \tag{3}$$

where d_{p} is the penetration depth, and c is the speed of light in free space.

The study investigates the impact of dielectric heating on changes in the properties of lead contaminants in planting soil. The investigation is facilitated by utilizing Eqs. (2) and (3), which describe temperature variations over time and depth of heat penetration into the soil, respectively. Essentially, electromagnetic fields are employed to transmit energy to lead-contaminated soil, inducing vibrations. Consequently, this process causes lead contaminants within the soil to move upward, accumulating on the upper electrode plate. It is noteworthy that lead-contaminated soil exhibits dielectric properties characterized by distinct loss values corresponding to both temperature and frequency.

2.3. Measurement of dielectric constant properties

The measurement of dielectric properties entails the use of various tools and equipment available within the same environment as shown in Fig. 3. These tools include an open-ended coaxial probe, an Agilent Technologies network analyzer (E5071C), a 50 Ω coaxial cable, and a computer equipped with software for analysis.

$$\varepsilon = \varepsilon' - j\varepsilon'' \tag{4}$$

where ε' is the dielectric constant and ε'' is the dielectric loss factor.

The relationship between the dielectric constant and dielectric loss is crucial in studying the dielectric properties of materials. This relationship indicates the efficiency of dielectric materials under various conditions. Measuring dielectric loss helps in understanding the amount of energy lost. Materials with low dielectric loss are more efficient because they lose less energy. Conversely, materials with high dielectric loss may be unsuitable for applications requiring stability and high efficiency. After testing with RF waves and examining the results by measuring the dielectric constant and dielectric loss, the tested material was found to exhibit a high dielectric constant and low dielectric loss. Therefore, it is highly efficient, retains energy well, and is highly suitable for practical applications.

The vector network analyzer (VNA) calibration process involved air, a shorting block, and deionized water, following the recommendations in [76]. The calibration and measurements were performed in a laboratory with an ambient temperature of 25 °C. Prior to initiating each measurement, the system was set up with a measurement range of 20 MHz to 10 GHz, utilizing a VNA configured with 1001 sampling points.

The complex relative permittivity is an indicator of a material's capacity to permit the passage of an electric field. It typically shows variations that are dependent on frequency when exposed to an external electric field. This frequency-dependent characteristic of complex permittivity can be explained by the Debye equation, which is formulated as follows [77]:

$$\varepsilon = \varepsilon_\infty + \frac{\varepsilon_s - \varepsilon_\infty}{1 + j\omega\tau} \tag{5}$$

where ε_s is the static dielectric constant, ε_∞ is the dielectric constant at high frequency, ω is the angular frequency, and τ is the relaxation time. Eq. (5) can be decomposed into dielectric constant ε', and dielectric loss factor ε'', expressed as Eqs. (6) and (7) [78], respectively:

$$\varepsilon' = \varepsilon_\infty + \frac{\varepsilon_s - \varepsilon_\infty}{1 + (j\omega\tau)^2} \tag{6}$$

$$\varepsilon'' = \frac{(\varepsilon_s - \varepsilon_\infty)}{1 + (j\omega\tau)^2} \tag{7}$$

2.4. Statistical analysis

To identify significant differences in dielectric properties among soil samples, a one-way ANOVA was conducted thrice using MATLAB version R2019a. The analysis employed a 5% significance level. The results indicated substantial differences in the dielectric properties across the soil samples tested.

3. Results and discussion

This section presents and analyzes the measured temperature data, dielectric properties, and corresponding statistical analysis results.

3.1. Influence of electric field intensity and temperature on the heating system performance

To investigate the influence of electric field intensity on temperature changes during RF heating, experiments were conducted at 112.5, 150, 225, and 450 kV/m. Soil samples contaminated with lead at concentrations of 200, 600, and 1000 mg/L were subjected to 9 kW of power for 30 min. Temperature measurements were recorded every minute using a U5857A infrared thermal imager from Keysight Technologies Inc., Santa Rosa, CA, USA [79]. Fig. 4 displays the distinctions in soil contamination at different lead concentrations and field intensities.

The analysis involved examining the time–temperature data derived from electric field strengths of 112.5, 150, 225, and 450 kV/m. Figs. 4–6 present the temperature versus time graphs for soils with high-, medium-, and low-moisture levels, respectively. In Figs. 4a–4d, it is evident that the temperature increases with electric field intensity. Over time, higher electric field intensities result in higher maximum temperatures, but this does not mean that a higher electric field strength always leads to continuously increasing temperatures. When heat reaches its limit or maximum point, the substance enters a state of equilibrium where the temperature does not rise further.

According to the measured results, the highest temperature of 109 °C is achieved at an electric field intensity of 450 kV/m after 5 min of RF heating. This outcome is attributed to the combined effects of high humidity and significant lead contamination in the soil, as shown in Fig. 4d.

Additionally, the three soil samples exhibit temperature variations corresponding to their lead concentrations (1000 mg/L > 600 mg/L > 200 mg/L). This indicates a correlation between the amount of lead in the soil and temperature, with higher lead amounts
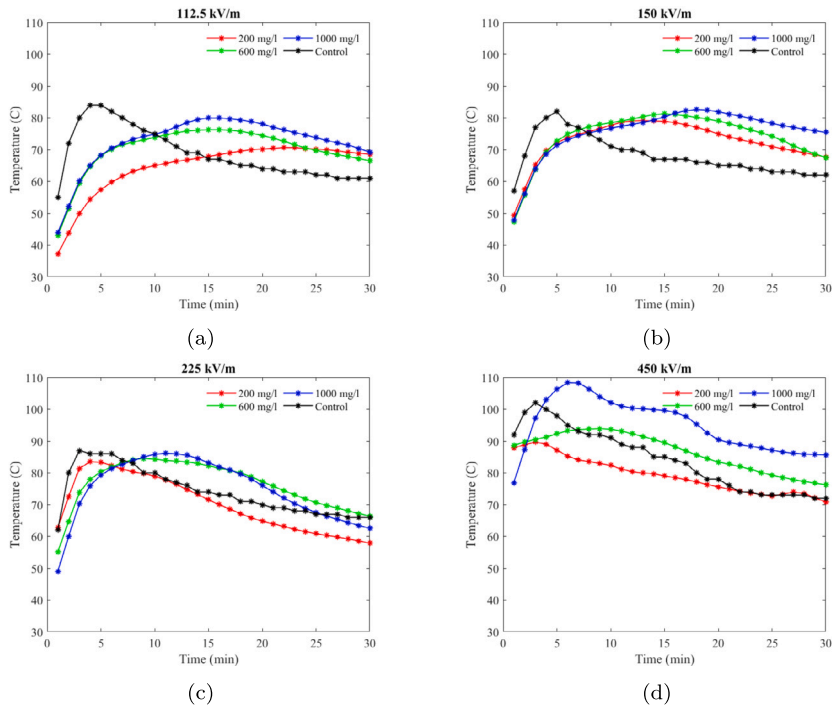
Fig. 4. Temperature differences in lead-contaminated soil with high humidity during RF heating at various electric field intensities: a) 112.5, b) 150, c) 225, and d) 450 kV/m.

Fig. 5. Temperature differences in lead-contaminated soil with medium humidity during RF heating at various electric field intensities: a) 112.5, b) 150, c) 225, and d) 450 kV/m.

Fig. 6. Temperature differences in lead-contaminated soil with low humidity during RF heating at various electric field intensities: a) 112.5, b) 150, c) 225, and d) 450 kV/m.
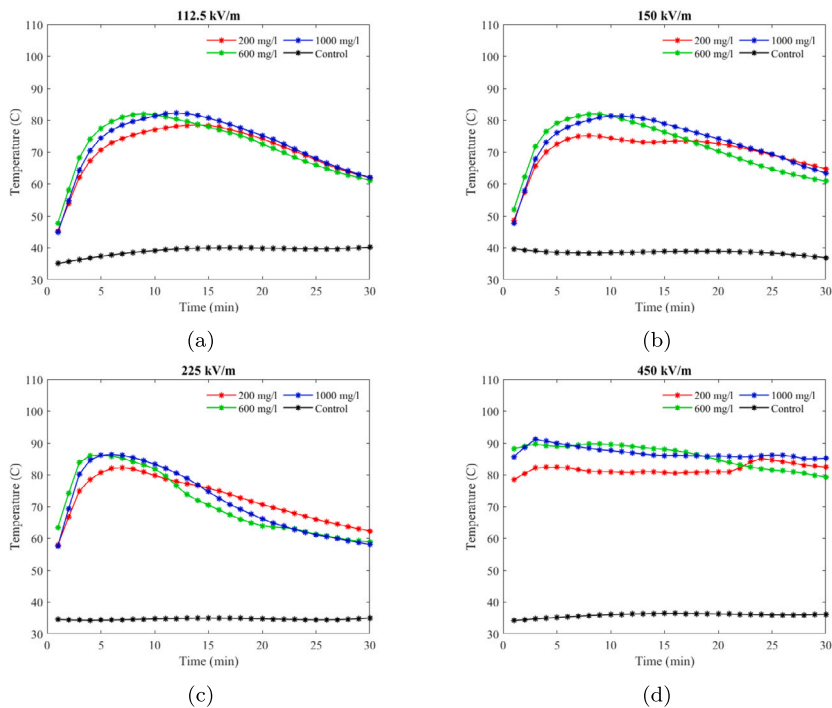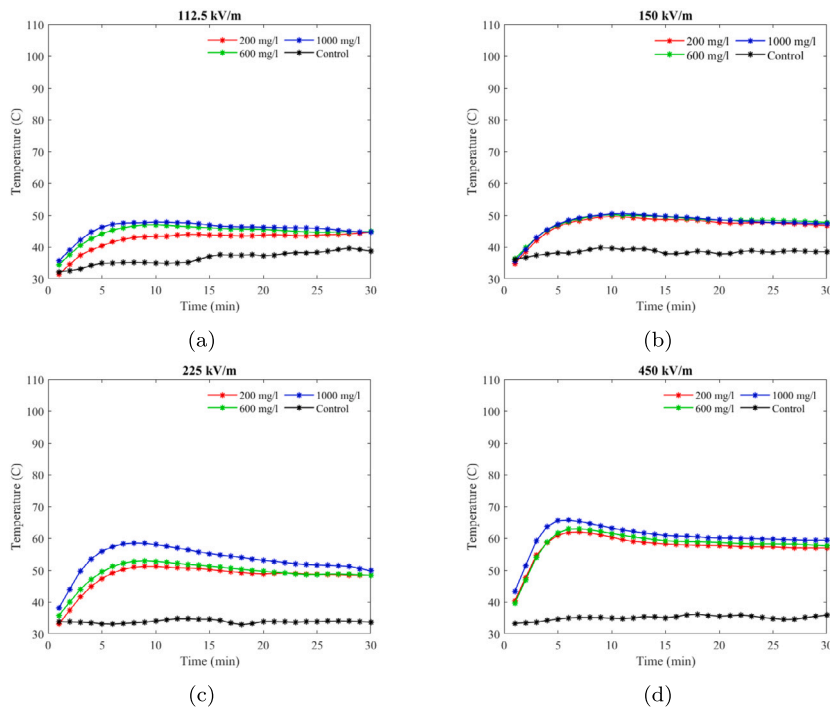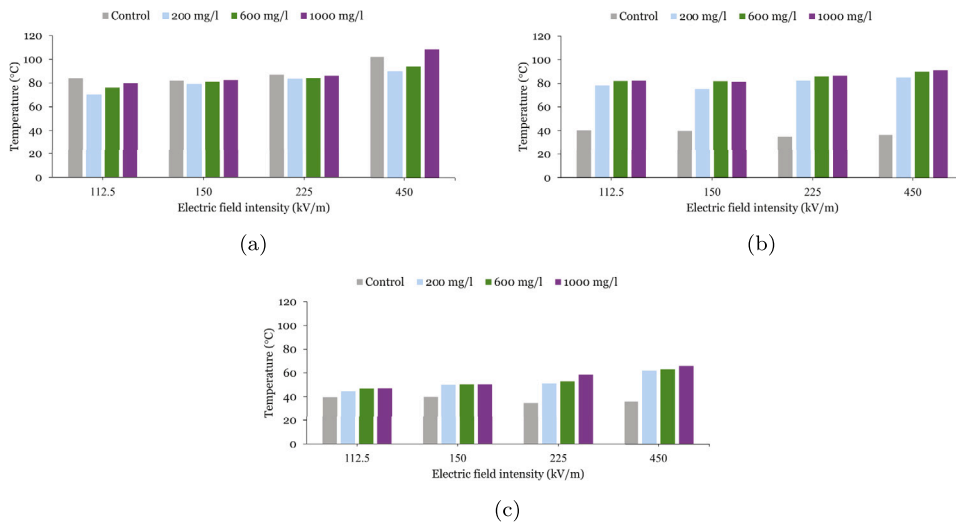

Fig. 7. Relationship between electric field intensity, soil temperature, and lead concentration under a) high-, b) moderate-, and c) low-humidity levels.

resulting in elevated temperatures. The findings indicate a complex interplay between electric field strength, soil lead content, and temperature, contributing to the understanding of how lead accumulation in soil may impact the temperature during the application process. RF heating with a high electric field intensity of 450 kV/m results in the highest temperatures in soils with the greatest lead accumulation, providing insights into theoretical principles and potential future developments in this field.

The measured results depicted in Figs. 5 and 6 indicate that temperature is influenced by electric field intensity. As the electric field intensity increases, the temperature also rises, similar to the trend in Fig. 4, but with a lower temperature value for soils with medium- and low-humidity levels. Additionally, control lines for the non-contaminated soil are plotted. It is shown that the high-humidity control lines have large values, similar to those observed in contaminated soil. Moreover, when examining dry soil under medium- and low-humidity levels, the control lines indicate lower temperatures, as shown in Figs. 4– 6.

The relationship between electric field intensity, soil temperature, and lead concentration is illustrated in Fig. 7. The temperatures of soil samples under varying electric field intensities and lead contamination levels (control, 200 mg/L, 600 mg/L, and 1000 mg/L)
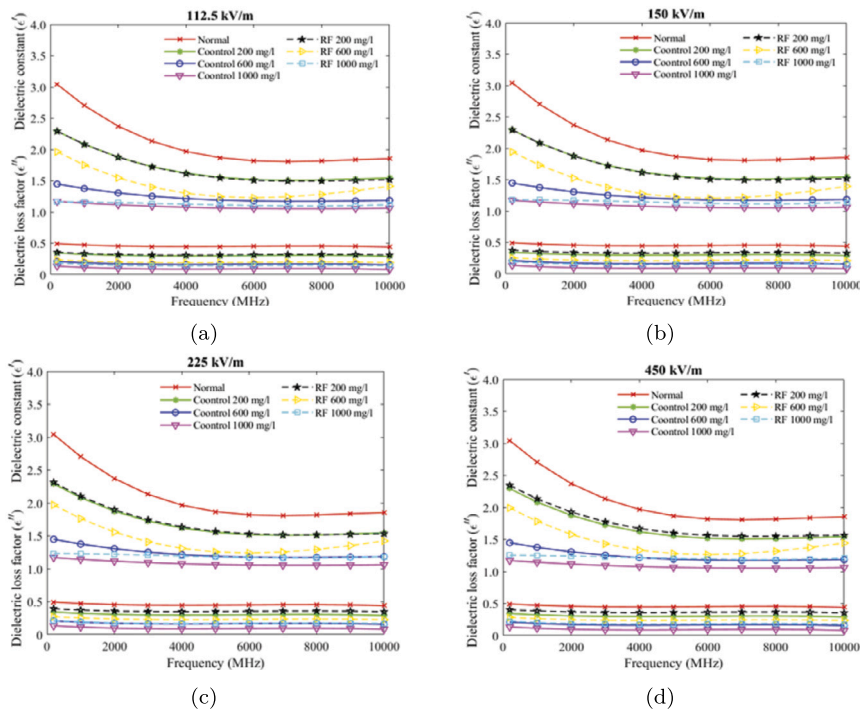
Fig. 8. Comparison of dielectric properties before and after RF heating for high-humidity soil. Dielectric constant and loss factor measurements at electric field intensities of (a) 112.5, (b) 150, (c) 225, and (d) 450 kV/m for lead-contaminated and uncontaminated soil.

across high-, moderate-, and low-humidity conditions are displayed. Under high humidity, the soil temperature rises with increasing electric field intensity, peaking at 1000 mg/L lead concentration. A similar trend is shown under moderate humidity; however, the overall temperature is lower. A consistent temperature increase is observed under low humidity, with the highest value occurring at 1000 mg/L and 450 kV/m, although the differences are less pronounced. The results indicate that temperature increases with both electric field intensity and lead concentration, impacting the soil dielectric properties and energy absorption.

3.2. Dielectric property measurement results

The dielectric constant and total dielectric loss factor were measured under high-, medium-, and low-humidity levels. Each condition involves two types of soil: untreated soil and soil treated with RF heat. The soil samples were contaminated with lead at concentrations of 200, 600, and 1000 mg/L. The dielectric constant measurements were conducted using various electric field intensities of 112.5, 150, 225, and 450 kV/m.

The collected data were statistically analyzed and used to create graphs in MATLAB, adjusting them to fit a polynomial curve. This curve aimed to closely represent the actual measured values, as depicted in Figs. 8– 10.

The graphs in Figs. 8–10 show the test results of lead-contaminated soil under the three different moisture conditions, revealing some interesting trends. These results were obtained by applying RF heating at electric field intensities of 112.5, 150, 225, and 450 kV/m under high-, medium-, and low-humidity conditions. In each condition, both RF-treated soil samples and normal (untreated) soil samples were analyzed to determine the impact of lead contamination.

The dielectric constants of seven soil samples were measured to facilitate comparisons under varying RF heating conditions. Non-contaminated soil exhibits the highest dielectric constant. Increasing lead contamination levels correlate with decreasing dielectric constant. This is due to the increased electrical conductivity within the material's lattice structure causing vibrations and gaps in the atom. This condition reduces the material's ability to store charge, ultimately lowering the dielectric constant. This phenomenon is well documented in the literature [80][81]. Furthermore, lead-contaminated soil subjected to RF heating shows an increase in the dielectric constant, which correlates with the electric field intensity.

Comparison of the three humidity levels reveals that under high-humidity conditions, the dielectric constant exhibits minimal changes with RF heating. This suggests that lead removal may be less effective in high-moisture soil. Conversely, in moderate- and low-humidity soils, a more significant change in the dielectric constant can be observed, particularly as the electric field intensity increases. These findings imply that lead-contaminated soil exhibits greater responsiveness to RF heating and lead may be effectively removed from soils with lower moisture content. However, the minimal variation in the dielectric constant in high-moisture soils indicates a potentially reduced impact of RF heating in those conditions.

Fig. 9. Comparison of dielectric properties before and after RF heating for medium-humidity soil. Dielectric constant and loss factor measurements at electric field intensities of (a) 112.5, (b) 150, (c) 225, and (d) 450 kV/m for lead-contaminated and uncontaminated soil.
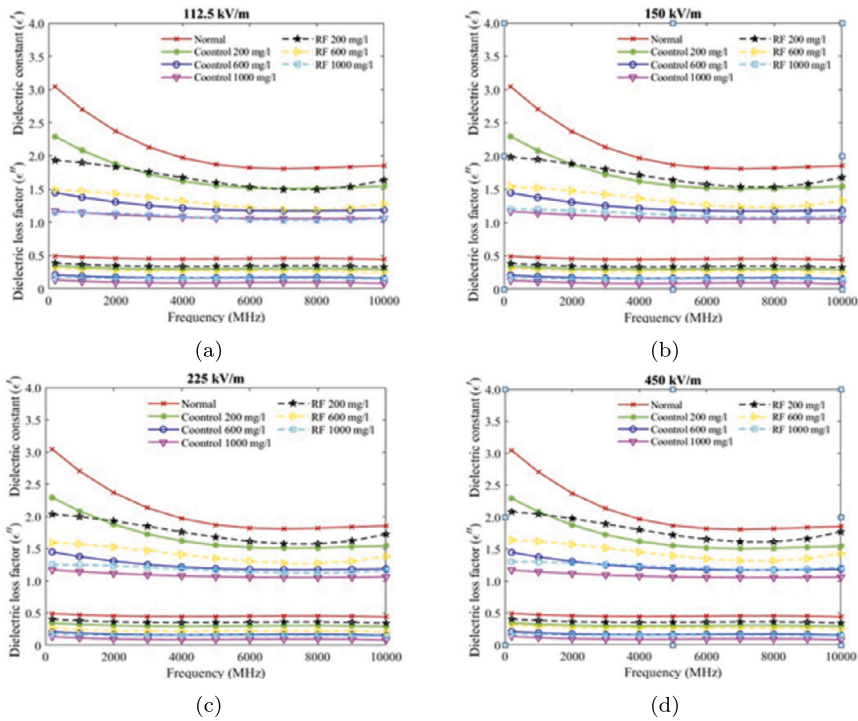

Fig. 10. Comparison of dielectric properties before and after RF heating for low-humidity soil. Dielectric constant and loss factor measurements at electric field intensities of (a) 112.5, (b) 150, (c) 225, and (d) 450 kV/m for lead-contaminated and uncontaminated soil.
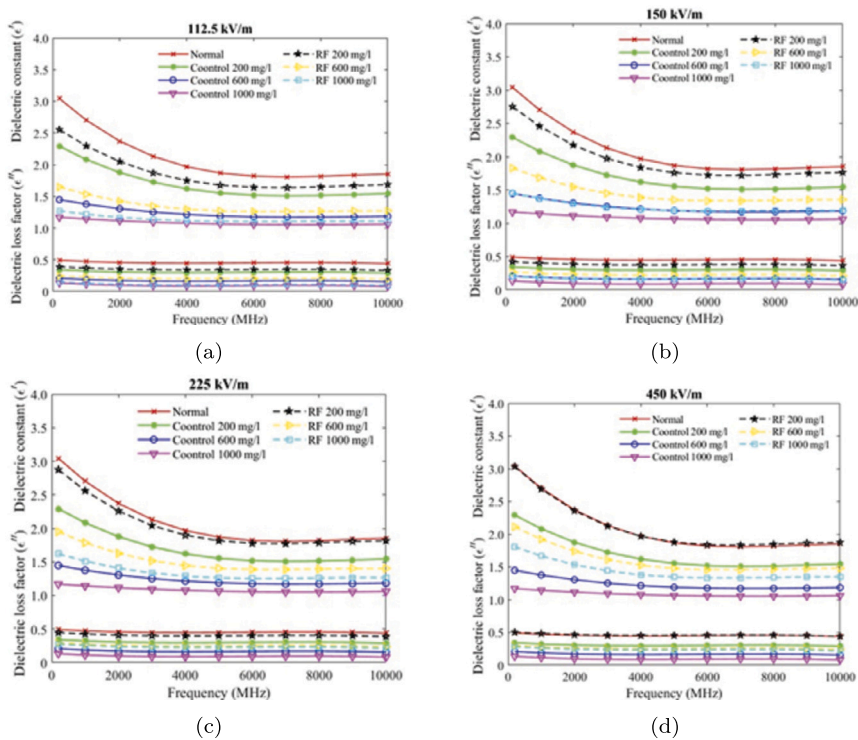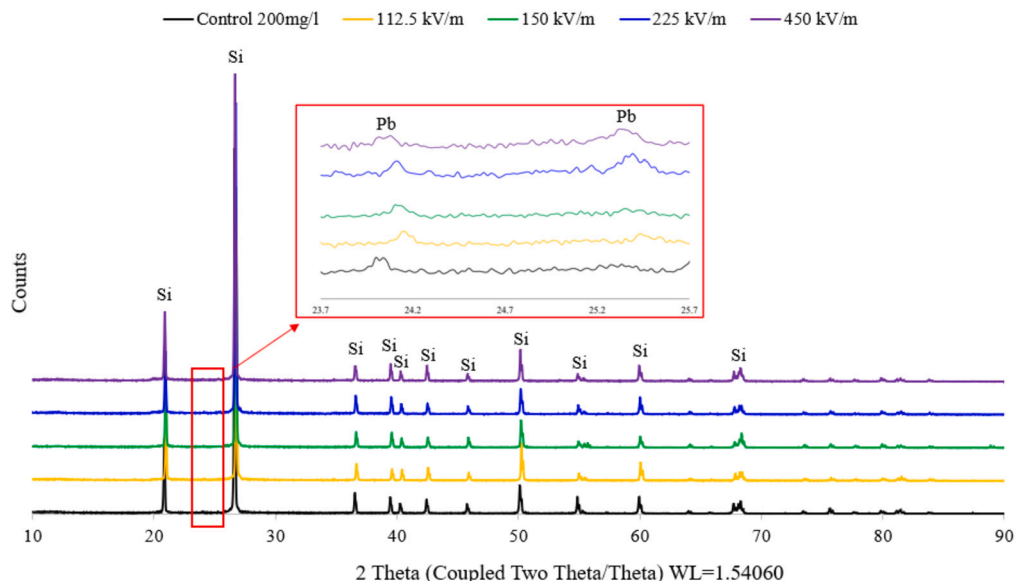
Fig. 11. XRD patterns of lead-contaminated soil samples at various electric field intensities, along with the control sample at 200 mg/L.

These test results demonstrate that the dielectric constant of lead- contaminated soil varies under different conditions, particularly with the intensity of the electric field applied during the RF heating process. This provides crucial insights into the mechanism of RF heating for lead removal from soil, highlighting the influence of soil moisture on the process effectiveness.

This research focuses on analyzing the dielectric properties of soil samples subjected to RF heating under various conditions. The study specifically examines soil moisture at three levels, namely, high, medium, and low, utilizing electric field intensities of 112.5, 150, 225, and 450 kV/m, as listed in Table 3. Statistical analysis reveals significant differences in the dielectric properties of the soil samples under each humidity condition and electric field intensity, particularly when compared with those of untreated or normal soil. The most notable differences can be observed at an electric field intensity of 450 kV/m, across all moisture conditions. These differences are particularly pronounced in the soil electrical conductivity. The observed variations, distinct from the properties of normal soil, clearly demonstrate the impact of electric field intensity on the dielectric properties of soil in varying humidity conditions.

The impact of frequency on the dielectric constant (ϵ') can be summarized as follows: when the frequency increases, ϵ' tends to decrease across soils with high-, medium-, and low-moisture levels. For instance, at a lead concentration of 200 mg/L, the dielectric constant at 0.2 GHz is 3.04, which decreases to 1.85 at 10 GHz. This trend is observable in all moisture conditions and at all lead concentrations. The effect of frequency on the dielectric loss factor (ϵ'') shows a similar trend: as the frequency increases, the dielectric loss factor decreases. For example, for soil with medium moisture at a lead concentration of 200 mg/L, the dielectric loss factor at 0.2 GHz is 0.70, decreasing to 0.41 at 10 GHz. Therefore, higher frequencies result in lower dielectric properties. This trend is exhibited in soils with high-, medium-, and low-moisture levels and at all lead concentrations. These observations are consistent with the general principles of dielectric physics, which indicate that as frequency increases, the molecules in the material have less time to align with the electric field, resulting in reduced dielectric constant and energy loss.

3.3. Post-heating soil quality and evaluation of lead removal efficiency

When removing lead from soil, factors such as current, voltage, and soil properties must be considered. However, the lead removal rate is the most important indicator for evaluating this technology's effectiveness. Therefore, achieving accurate measurements of the lead removal rate is of utmost importance. Additional results were collected using lead-contaminated soil samples with a concentration of 200 mg/L, exposed to electric field strengths of 112.5, 150, 225, and 450 kV/m, along with unheated soil as control samples (contaminated with lead (II) acetate trihydrate at 200 mg/L). These samples were analyzed using X-ray diffraction (XRD). Fig. 11 shows the XRD patterns of lead-contaminated soil samples at various electric field intensities, alongside the control sample at 200 mg/L. The analysis reveals that lead does not react with silica and remains in the form of lead acetate. The observed pattern confirms lead contamination and indicates that RF heating facilitates lead ion migration, aiding in soil remediation. The overall effectiveness of RF heating lies in its ability to selectively target lead contaminants while preserving the soil structural integrity. This optimization is achieved by addressing both the electrical and chemical aspects of the remediation process.

Table 4 compares the composition of soil samples in glass dishes, focusing on silicon, lead, and other components, analyzed using the XRF technique under different conditions and electric field strengths. A clear trend in lead removal rates is evident: as the electric field intensity increases, the lead removal efficiency improves. Specifically, the average removal rates are 15.385% at 112.5 kV/m, 30.769% at 150 kV/m, 42.308% at 225 kV/m, and 46.154% at 450 kV/m (the highest rate). These data suggest that higher electric field strengths significantly enhance the electrostatic forces acting on lead ions, thereby increasing their removal from the soil. In

Table 3
Dielectric Properties of Lead-Contaminated Soil Samples at Various Concentrations.

Soil conditions	Substance concentration (mg L⁻¹)	Frequency GHz	Normal		112.5 kV/m		150 kV/m		225 kV/m		450 kV/m	
			ϵ'	ϵ''	ϵ'	ϵ''	ϵ'	ϵ''	ϵ'	ϵ''	ϵ'	ϵ''
Height humidity	200	0.2	3.04	0.49	1.93	0.48	1.98	0.48	2.03	0.48	2.08	0.49
		1.0	2.70	0.47	1.89	0.46	1.94	0.46	1.99	0.46	2.04	0.46
		3.0	2.13	0.44	1.75	0.43	1.80	0.43	1.84	0.43	1.89	0.43
		6.0	1.82	0.45	1.53	0.43	1.57	0.43	1.61	0.43	1.65	0.43
		10.0	1.85	0.44	1.63	0.42	1.68	0.41	1.72	0.41	1.77	0.41
	600	0.2	3.04	0.49	1.49	0.31	1.54	0.31	1.59	0.31	1.64	0.31
		1.0	2.70	0.47	1.47	0.29	1.52	0.29	1.57	0.29	1.61	0.29
		3.0	2.13	0.44	1.37	0.26	1.42	0.26	1.47	0.26	1.51	0.26
		6.0	1.82	0.45	1.21	0.27	1.26	0.27	1.30	0.27	1.34	0.27
		10.0	1.85	0.44	1.27	0.25	1.32	0.25	1.37	0.25	1.42	0.25
	1000	0.2	3.04	0.49	1.51	0.16	1.20	0.16	1.25	0.16	1.30	0.16
		1.0	2.70	0.47	1.47	0.16	1.19	0.16	1.24	0.16	1.29	0.16
		3.0	2.13	0.44	1.11	0.15	1.16	0.15	1.21	0.15	1.26	0.15
		6.0	1.82	0.45	1.04	0.15	1.09	0.15	1.14	0.15	1.19	0.15
		10.0	1.85	0.44	1.06	0.14	1.10	0.14	1.16	0.14	1.21	0.14
Medium humidity	200	0.2	3.04	0.49	2.29	0.35	2.29	0.37	2.31	0.39	2.34	0.40
		1.0	2.70	0.47	2.08	0.33	2.08	0.35	2.10	0.37	2.13	0.38
		3.0	2.13	0.44	1.72	0.31	1.72	0.32	1.74	0.34	1.77	0.35
		6.0	1.82	0.45	1.50	0.31	1.50	0.33	1.52	0.35	1.56	0.36
		10.0	1.85	0.44	1.51	0.31	1.51	0.32	1.53	0.34	1.56	0.35
	600	0.2	3.04	0.49	1.96	0.23	1.94	0.25	1.97	0.27	1.99	0.28
		1.0	2.70	0.47	1.75	0.21	1.73	0.23	1.76	0.25	1.78	0.26
		3.0	2.13	0.44	1.39	0.18	1.37	0.20	1.40	0.22	1.43	0.23
		6.0	1.82	0.45	1.22	0.19	1.20	0.21	1.23	0.23	1.26	0.24
		10.0	1.85	0.44	1.41	0.14	1.39	0.20	1.42	0.22	1.44	0.23
	1000	0.2	3.04	0.49	1.16	0.18	1.18	0.19	1.23	0.21	1.25	0.22
		1.0	2.70	0.47	1.15	0.16	1.17	0.17	1.22	0.19	1.24	0.20
		3.0	2.13	0.44	1.13	0.13	1.15	0.14	1.20	0.16	1.22	0.17
		6.0	1.82	0.45	1.10	0.14	1.12	0.15	1.17	0.17	1.19	0.18
		10.0	1.85	0.44	1.11	0.14	1.13	0.14	1.18	0.16	1.20	0.17
Low humidity	200	0.2	3.04	0.49	2.55	0.35	2.75	0.37	2.87	0.38	3.03	0.40
		1.0	2.70	0.47	2.29	0.33	2.45	0.35	2.56	0.36	2.69	0.38
		3.0	2.13	0.44	1.87	0.31	1.97	0.32	2.04	0.34	2.12	0.35
		6.0	1.82	0.45	1.64	0.31	1.72	0.33	1.77	0.34	1.83	0.36
		10.0	1.85	0.44	1.68	0.30	1.76	0.32	1.81	0.33	1.87	0.35
	600	0.2	3.04	0.49	1.64	0.22	1.82	0.23	1.95	0.25	2.11	0.26
		1.0	2.70	0.47	1.53	0.20	1.68	0.21	1.78	0.23	1.92	0.24
		3.0	2.13	0.44	1.34	0.17	1.45	0.19	1.51	0.20	1.60	0.22
		6.0	1.82	0.45	1.25	0.18	1.18	0.19	1.38	0.21	1.45	0.22
		10.0	1.85	0.44	1.27	0.17	1.35	0.18	1.40	0.20	1.47	0.21
	1000	0.2	3.04	0.49	1.27	0.14	1.45	0.16	1.62	0.17	1.80	0.19
		1.0	2.70	0.47	1.21	0.12	1.37	0.14	1.51	0.15	1.66	0.17
		3.0	2.13	0.44	1.13	0.10	1.24	0.11	1.33	0.13	1.44	0.14
		6.0	1.82	0.45	1.10	0.10	1.18	0.12	1.25	0.13	1.33	0.15
		10.0	1.85	0.44	1.10	0.09	1.19	0.11	1.24	0.12	1.35	0.14

Table 4
Composition of soil samples analyzed by X-ray fluorescence at various electric field strengths.

Type	Control Normal	Control 200 mg/L	112.5 kV/m	150 kV/m	225 kV/m	450 kV/m
Si (%)	93.95	93.80	93.303	93.170	88.725	87.259
Pb (%)	-	0.026	0.022	0.018	0.015	0.014
Other (%)	6.05	6.174	6.812	6.812	11.260	12.727

addition, the changes in the soil physicochemical properties under different electric field strengths alter the distribution of silicon and other elements.

The quality of treated contaminated soil was evaluated. Fig. 11 displays soil contaminated with lead (II) acetate trihydrate (at a concentration of 200 mg/L) adhering to the upper electrode plate after RF heating. This adhesion is due to the movement of heavy metal (lead) ion particles within the soil, driven by the high-intensity electric fields between the electrodes. As the electric field traverses the gap between electrodes, the heavy metal ion particles are subjected to an electrostatic force, drawing them toward the
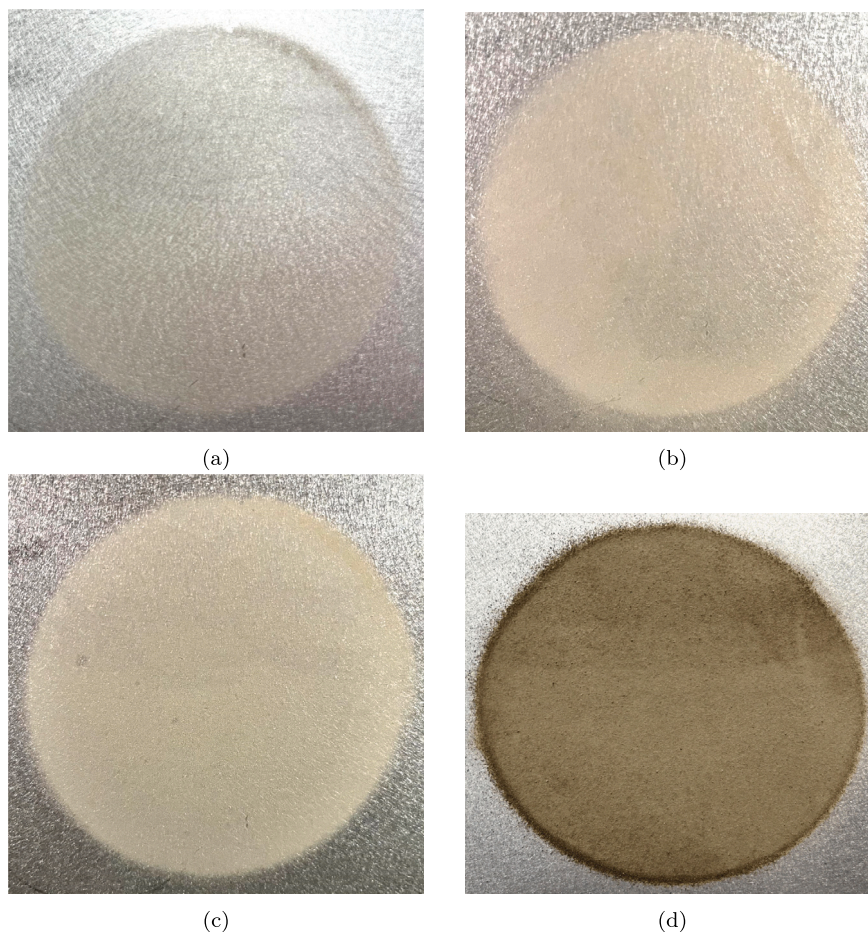
Fig. 12. Soil contaminated with lead (II) acetate trihydrate adhering to the upper electrode plate after RF heating at electric field intensities of (a) 112.5, (b) 150, (c) 225, and (d) 450 kV/m.

opposite plate. Observations reveal that the soil layer on the top plate progressively thickens with increasing electric field intensity. This phenomenon correlates with the findings for the dielectric constant and dielectric loss factor measurements presented in Fig. 10d. The dielectric value of the soil sample contaminated with lead at 200 mg/L approaches that of normal soil samples as the electric field intensity increases. The sample that adhered to the top plate under RF heating at 450 kV/m, as shown in Fig. 12d, was analyzed using XRF. This condition was chosen because the dielectric constant measurement indicated that it closely matched the dielectric constant of uncontaminated soil. The XRF analysis indicates that the sample contains lead with a mass of 0.013%, indicating effective migration and accumulation of lead particles on the electrode.

4. Conclusions

This paper presents a comprehensive study on the effectiveness of RF heating in mitigating lead contamination in soil. The study involved assessing the reduction of lead levels by measuring the dielectric constant, using lead (II) acetate trihydrate as a soluble indicator. The experiment was meticulously conducted on soil samples with varying lead concentrations of 200, 600, and 1000 mg/L under different electric field intensities (112.5, 150, 225, and 450 kV/m). Additionally, the soil samples were categorized based on their moisture content, namely, high-, medium-, and low-humidity levels, to determine the influence of moisture on the remediation process. The study revealed an inverse correlation between dielectric constant and lead concentration in soil samples. However, RF heating increased the dielectric constant, indicating effective lead removal. At 450 kV/m, XRF analysis showed a maximum removal rate of 46.154%. XRD confirmed that lead remained as lead acetate, demonstrating the potential of RF heating for broader contaminant remediation. The study found an inverse correlation between dielectric constant and lead concentration in soil samples. However, when these contaminated soils were subjected to RF heating, the dielectric constant remarkably increased with increasing electric field intensity, indicating the effectiveness of RF heating in lead removal. At 450 kV/m, the XRF analysis showed removal rates peaking at 46.154%. The XRD analysis confirmed that lead remained as lead acetate, demonstrating the efficacy of RF heating for lead remediation in soil and suggesting its potential for treating other contaminants.

Moreover, the impact of soil moisture content was significant. Soils with high humidity showed minimal changes in dielectric constant when subjected to RF heating, implying a lesser efficiency in lead removal under this condition. In stark contrast, soils with medium- and low-humidity levels exhibited more substantial changes in their dielectric constants, indicating that RF heating is more effective in these environments. The research conclusively demonstrated that, when subjected to RF heating, the dielectric constant of lead-contaminated soil responds differently under varying conditions of electric field intensity and soil moisture. This variability provides crucial insights into the mechanism of RF heating in soil lead removal, especially under different moisture conditions. The study conclusively highlighted the efficacy of RF heating as a feasible method for mitigating lead pollution in soils, particularly in environments characterized by medium- to low-moisture levels. It is suggested that forthcoming investigations should explore the broader applicability of the RF treatment methodology across various substrates, including aquatic systems. Additionally, extending its remediation capabilities to a diverse array of heavy metals—such as silver, cadmium, chromium, copper, mercury, nickel, and zinc—as well as crude oils would be valuable.

Funding statement

Additional information

No additional information is available for this paper.

CRediT authorship contribution statement

Samroeng Santalunai: Writing – review & editing, Writing – original draft, Visualization, Validation, Software, Methodology, Investigation, Formal analysis, Data curation, Conceptualization. **Jariya Pakprom:** Writing – review & editing, Writing – original draft, Visualization, Validation, Software, Methodology, Investigation, Formal analysis, Data curation, Conceptualization. **Weerawat Charoensiri:** Visualization, Software, Data curation, Conceptualization. **Chanchai Thongsopa:** Writing – review & editing, Writing – original draft, Validation, Supervision, Resources, Project administration, Methodology, Formal analysis, Data curation, Conceptualization. **Thanaset Thosdeekoraphat:** Conceptualization. **Pisit Janpangngern:** Writing – review & editing, Writing – original draft, Visualization, Validation, Software, Methodology, Investigation, Formal analysis, Data curation, Conceptualization. **Teerapon Yodrot:** Methodology, Conceptualization. **Nuchanart Santalunai:** Writing – review & editing, Writing – original draft, Visualization, Validation, Supervision, Project administration, Methodology, Investigation, Formal analysis, Data curation, Conceptualization. **Samran Santalunai:** Writing – review & editing, Writing – original draft, Visualization, Validation, Supervision, Resources, Project administration, Methodology, Investigation, Funding acquisition, Formal analysis, Data curation, Conceptualization.

Declaration of competing interest

The authors declare the following financial interests/personal relationships which may be considered as potential competing interests: Samran Santalunai reports financial support was provided by Suranaree University of Technology (SUT), Research and Development Fund under Grant IRD7-715-67-12-12. If there are other authors, they declare that they have no known competing financial interests or personal relationships that could have appeared to influence the work reported in this paper.

References

[1] V.A. Reddy, C.H. Solanki, S. Kumar, K.R. Reddy, Y.J. Du, Stabilization/solidification of zinc and lead-contaminated soil using limestone calcined clay cement (lc3): An environmentally friendly alternative, IEEE Trans. Sustain. Energy 12 (2020) 3725–3733.

[2] F. Zabel, D. Ruth, M.S. Julia, S. Ralf, M. Wolfram, V. Tomáš, Global impacts of future cropland expansion and intensification on agricultural markets and biodiversity, Nat. Commun. 10 (2019) 2844.

[3] G. Shreya, G. Mayuri, D.V.H. Eric, P.D. Alok, Proteomic insights into lysinibacillus sp.-mediated biosolubilization of manganese, Environ. Sci. Pollut. Res. Int. 28 (2021) 40249–40263.

[4] A. Umair, A. Huma, S. Hafsa, B. Muhammad, M. Hafiz, M. Shahzad, S. Muhammad, A. Muhammad, H. Afaq, R. Nova, R. Saravanan, M. Muhammad, S.K. Kuan, Remediation techniques for elimination of heavy metal pollutants from soil: a review, Environ. Res. 212 (2022) 113918.

[5] T. Banismita, D. Akankshya, P.D. Alok, Detection of environmental microfiber pollutants through vibrational spectroscopic techniques: recent advances of environmental monitoring and future prospects, Crit. Rev. Anal. Chem. 12 (2022) 1–11.

[6] S. Muhammad, K. Sana, A. Ghulam, N. Naeem, S. Muhammad, A. Muhammad, S. Muhammad, D. Camille, Heavy metal stress and crop productivity 1 (2015) 1–25.

[7] B.S. Ismail, K. Farihah, J. Khairiah, Bioaccumulation of heavy metals in vegetables from selected agricultural areas, Bull. Environ. Contam. Toxicol. 74 (2005) 320–327.

[8] M. Amir, N.M. Sepideh, L.N. Moslem, T. Ali, A. Ali, F. Maryam, M. Mohammad, Probabilistic risk assessment of soil contamination related to agricultural and industrial activities, Environ. Res. 203 (2022) 111837.

[9] A.W. Raymond, E.O. Felix, General optimization technique for high-quality community detection in complex networks, in: Risks and Best Available Strategies for Remediation, vol. 2011, 2011, p. 20.

[10] P. Bhunia, Environmental toxicants and hazardous contaminants: Recent advances in technologies for sustainable development, J. Hazard., Toxic, Radioact. Waste 21 (2017) 02017001.

[11] H. Abdelmajid, E.R. Taoufik, N. Mohamed, B. Said, The effect of cd, zn, and fe on seed germination and early seedling growth of wheat and bean, Ekológia (Bratisl.) 35 (2016) 213–223.
[12] M. Minodora, O. Marilena, I.B. Raluca, The effect of heavy metals on mite communities (acari: gamasina) from urban parks - Bucharest, Romania, Environ. Eng. Manag. J. 17 (2018) 2071–2081.
[13] V. Narcisa, M.H. Raluca, I.S. Andrei, R. Lacramioara, F.K. Ildikó, B. Noureddine, F. Lidia, New evidence of the enhanced elimination of a persistent drug used as a lipid absorption inhibitor by advanced oxidation with UV-a and nanosized catalyst, Catalysts 9 (2019) 761.
[14] Z.I. Muhammad, J.S. Kyu, W.A. Muhammad, K.L. Ju, Toxic effects of lead on plants: integrating multi-omics with bioinformatics to develop pb-tolerant crops, Planta 259 (2023) 44.
[15] M.T. Iqbal, M.Z. Mahmood, A. Firdous, Influence of cadmium toxicity on germination and growth of some common trees, Pak. J. Sci. Ind. Res. 34 (1991) 140–142.
[16] M. Aslam, A. Aslam, M. Sheraz, B. Ali, Z. Ulhassan, U. Najeeb, W. Zhou, R.A. Gill, Lead toxicity in cereals: Mechanistic insight into toxicity mode of action and management, Front. Plant Sci. 11 (2021) 587785.
[17] S. Babar, T. Mohsin, C. Zhao, R. Abdul, A.C. Sardar, S. Anket, S. He, U.R. Shams, Z. Dong, Role of 24-epibrassinolide (ebl) in mediating heavy metal and pesticide induced oxidative stress in plants: a review, Ecol. Environ. Saf. 147 (2018) 935–944.
[18] Q. Sadia, K. Ibrar, M. Ke, Z. Yangguo, P. Changsheng, A review on remediation technologies for heavy metals contaminated soil, Cent. Asian J. Environ. Sci. Technol. Innov. 1 (2020) 21–29.
[19] W. Zebin, C. Yihui, L. Xiaoqing, R. Haiyu, H. Zhujian, Remediation of heavy metal contaminated farmland soil by biodegradable chelating agent glda, Appl. Sci. 12 (2022) 9277.
[20] G. Resmi, S.G. Thampi, S. Chandrakaran, Heavy metal removal from contaminated soil using soil washing techniques, Nat. Environ. Pollut. Technol. 22 (2023) 129–138.
[21] L. Hongqiang, C. Pan, W. Hongbin, Y. Yaohui, W. Yulun, Remediation of cu-, zn-, and pb-contaminated soil using different soil washing agents: Removal efficiencies and mechanisms, Water Air Soil Pollut. 234 (2023) 476.
[22] Z. Xiaomei, P. Shirong, O. Ting, L. Jinyi, G. Guoshu, W. Guiyin, P. Xiaoxun, X. Yulin, J. Lulu, L. Yongxia, Response of microbiomes with different abundances to removal of metal fractions by soil washing, Ecotoxicol. Environ. Saf. 242 (2022) 113862.
[23] S.J. Lee, E.L. Myoung, W.C. Jae, H.P. Jin, Y.H. Keun, I.J. Gee, Immobilization of lead from pb-contaminated soil amended with peat moss, J. Chem. 2013 (2013) 509520.
[24] L. Mingxuan, H. Renjie, F. Qiang, L. Tianxiao, Z. Shoujie, S. Anshuang, Long-term immobilization of cadmium and lead with biochar in frozen-thawed soils of farmland in china, Environ. Pollut. 313 (2022) 120143.
[25] W. Yazhou, T. Renhao, Z. Li, L. Jie, W. Xudong, H. Rong, Y. Fan, H. Xinsheng, Z. Wenkun, Heavy metal fixation of lead-contaminated soil using morchella mycelium, Environ. Pollut. 289 (2021) 117829.
[26] Y. Zhihui, G. Hangyuan, H. Fangshu, R. Eveliina, Y. Weichun, L. Qi, Z. Feiping, Iron-doped hydroxyapatite for the simultaneous remediation of lead-, cadmium- and arsenic-co-contaminated soil, environmental pollution, Environ. Pollut. 312 (2022) 119953.
[27] J.C. Rojas-Montes, V.J. Martínez-Gómez, J.C. Fuentes-Aceituno, S. Valle-Cervantes, B.P. Gómez-Lozano, Q.L. Quiñones-Rosales, Maximum electrodeposition capacity of pb on a stainless-steel cathode using a galvanostatic regime, Int. J. Environ. Sci. Technol. 20 (2023) 13259–13266.
[28] R. Vemi, J.E. Agus, S. Muhayatun, S. Mahrus, F. Laili, P. Wisnu, Dissolved lead removal from soil-washing process using electrocoagulation, Environ. Res., Eng. Manag. 79 (2023) 75–84.
[29] S. Ximing, Z. Lin, H. Menglu, H. Ju, L. Xianwei, C. Daying, L. Jiashu, In-situ thermal conductive heating (tch) for soil remediation: A review, J. Environ. Manag. 351 (2023) 119602.
[30] A. Dinesh, A. Amit, B. Renu, P. Vishal, K. Sunil, Enhancement in phytoremediation efficiency of tagetus erecta with the application of nano-scale zero valent iron (nzvi) for the restoration of lead contaminated soil: an approach toward sustainability, Water Air Soil Pollut. 234 (2023) 535.
[31] A. Bhagwat, C.S.P. Ojha F.ASCE, A. Pant, R. Kuma, Interaction among heavy metals in landfill leachate and their effect on the phytoremediation process of indian marigold, J. Hazard., Toxic, Radioact. Waste 27 (2023) 04022039.
[32] X. Yao, E. Saikawa, S. Warner, P.E. D'Souza, P.B. Ryan, D.B. Barr, Phytoremediation of lead-contaminated soil in the westside of atlanta, GeoHealth 7 (2023) 12.
[33] R.S. Gilan, Y. Parvizi, E. Pazira, F. Rejali, Bioremediation of petroleum-contaminated soil in arid region using different arid-tolerant tree, shrub, and grass plant species with bacteria, IEEE Int. J. Environ. Sci. Technol. 19 (2022) 11879–11890.
[34] H. Bisht, N. Kumar, Characterization and evaluation of the nickel-removal capacity of kluyvera cryocrescens m7 isolated from industrial wastes, Pollution 9 (2023) 1059–1073.
[35] M.Y. Asunmo, T.A. Ogunnusi, O.B. Akpor, Heavy metal tolerance and removal efficiencies by soil bacterial strains: Effects of carbon and nitrogen sources, Open Biotechnol. J. 17 (2023) 1874–0707/23.
[36] N. Zhu, B. Zhang, Q. Yu, Genetic engineering-facilitated coassembly of synthetic bacterial cells and magnetic nanoparticles for efficient heavy metal removal, ACS Appl. Mater. Interfaces 12 (2020) 22948–22957.
[37] Y. Fangming, G. Tiantian, W. Jiayu, T. Chijian, L. Songying, C. Yuyuan, S. Yanlan, M. Kehui, L. Jiangming, L. Xin, L. Yi, Cafe-layered double hydroxide corn straw biochar reduced heavy metal uptake by brassica campestris L. and ipomoea aquatic F.: Rhizosphere effects and oxidative stress alleviation, ACS Appl. Mater. Interfaces 330 (2023) 117227.
[38] S.A. Nosrati, A. Negahdar, H. Negahdar, M. Siavoshnia, The effect of heavy metal on the static and dynamic performances of clay sand, IEEE J. Environ. Eng. 150 (2023) 04023095.
[39] S.A. Nosrati, A. Negahdar, H. Negahdar, M. Siavoshnia, Efficient removal of cd (ii) and pb (ii) from aqueous solution using biochars derived from food waste, Environ. Sci. Pollut. Res. 30 (2023) 122364–122380.
[40] T. Shuai, G. Xueliu, Y. Qiuyu, Y. Fei, L. Wenjian, G. Zilin, Z. Xin, Y. Yuan, F. Yuqing, B. Rongjun, W. Yan, Z. Xuhui, L. Lianqing, P. Genxing, Efficient removal of cd (ii) and pb (ii) from aqueous solution using biochars derived from food waste, Environ. Sci. Pollut. Res. 30 (2023) 122364–122380.
[41] T. Dagnew, Z. Bantie, Process optimization of cr (vi) removal from aqueous solution using activated orange peel for treatment of tannery wastewater, Ethiop. J. Sci. Technol. 16 (2023) 51–75.
[42] M. Alkhatib, O. Ayyad, R. Tbakhi, M. Qurie, A comparative study for lead removal by pure calcite and a natural calcitic soil sample, Int. J. Environ. Sci. Technol. 20 (2023) 12243–12250.
[43] A. Temoor, N. Muhammad, Q. Yetong, X. Shengchun, Y. Yanlai, A.M. Hafiza, M. Natasha, R. Muhammad, L. Bin, Q. Xingjiang, Dynamic crosstalk between silicon nanomaterials and potentially toxic trace elements in plant-soil systems, Ecotoxicol. Environ. Saf. 264 (2023) 115422.
[44] A. Horablaga, B. Lixandru, M. Petrovici, A.-A. Sinitean, A. Marin, F. Morariu, Use of benthic macroinvertebrates in the diagnosis of bega river water quality and self-purification process, Environ. Eng. Manag. J. 19 (2020) 505–510.
[45] F.C. Staff, B. Adam, China releases the standard for maximum levels of contaminants in foods, Tech. rep., The National Health Commission (NHC), 2023.
[46] S. Kotchapradit, T. Thosdeekoraphat, S. Santalunai, C. Thongsopa, Overlapping community detection via bounded nonnegative matrix tri-factorization, in: Proceedings of the Asia-Pacific Microwave Conference, 2018, pp. 1474–1476.
[47] P. Saeung, S. Santalunai, T. Thosdeekoraphat, C. Thongsopa, Improved efficiency of insect pest control system by sspa, in: International Conference on Industrial Engineering and Applications, 2018, pp. 179–183.
[48] T. Thosdeekoraphat, K. Tanthai, K. Lhathum, S. Kotchapradit, S. Santalunai, C. Thongsopa, The design of a large-scale induction heating power source for organic waste digesters to produce fertilizer, Energies 16 (2023) 16052123.

[49] A. Rattananamlom, S. Kotchapradit, S. Santalunai, T. Thosdeekoraphat, P. Moungnoul, C. Thongsopa, Design of high power transmission line transformer for rf heating generator, in: International Symposium on Antennas and Propagation, 2018, p. 2.

[50] N. Santalunai, S. Santalunai, P. Meesawad, C. Tongsopa, S. Santalunai, Plus-shape of mushroom-like ebg with square microstrip emitter to expand the working space in dielectric heating applications, J. Intell. Fuzzy Syst. 16 (2021) 189–200.

[51] S.S.T. Seehanan, N. Fhafhiem, P. Krachodnok, Analysis of electric fields distribution by using ebg structure for dielectric heating applications, in: 4th International Conference on Engineering, Applied Sciences, and Technology: Exploring Innovative Solutions for Smart Societies, 2018, pp. 1–4.

[52] N. Poungprakhon, C. Thongsopa, S. Santalunai, T. Thosdeekoraphat, N. Santalunai, P. Chaipanya, The study of water reconditioning using magnetic field for plant industry, Prz. Elektrotech. 99 (2023) 59–64.

[53] R. Noyes, Handbook of Pollution Control Process, Noyes Publications, 1991.

[54] E. Jordan, K. Balmain, Electromagnetic Waves and Radiating Systems, Electromagnetic Heating, Prentice-Hall, 1968.

[55] P. Neelakanta, RF Heating in Soil Remediation, in: Handbook of Electromagnetic Materials: Monolithic and Composite Versions and Their Applications, CRC Press, 1995.

[56] A. Metaxas, R. Meredith, RF Heating in Soil Remediation, in: Handbook of Electromagnetic Materials: Monolithic and Composite Versions and Their Applications, Peter Peregrinus Ltd, 1983.

[57] D. Pozar, Microwave Engineering, 4th Edition, Wiley, 2011.

[58] S. Nelson, Heating of materials by radio-frequency electric fields, IEEE Trans. Dielectr. Electr. Insul. 10 (2003) 811–821.

[59] W. Ge, B. Zhang, Application of radio frequency heating technology in the treatment of contaminated soil, Proc. Environ. Sci. 16 (2012) 337–343.

[60] Z. Liu, S. Liu, Y. Cai, W. Fang, Electrical resistivity characteristics of diesel oil-contaminated kaolin clay and a resistivity-based detection method, Environ. Sci. Pollut. Res. 22 (2015) 8216–8223.

[61] R. Zaharieva, Y. Kancheva, K. Kamenov, V. Tomov, V. Lyubomirova, Challenges in using handheld xrfs for in situ estimation of lead contamination in buildings, Processes 10 (2022) 839.

[62] A. Gholamhosseini, M. Banaee, A. Zeidi, C. Multisanti, C. Faggio, Individual and combined impact of microplastics and lead acetate on the freshwater shrimp (caridina foss arum): biochemical effects and physiological responses, J. Contam. Hydrol. 262 (2024) 104325.

[63] M.K. Zhang, Z.Y. Liu, H. Wang, Use of single extraction methods to predict bioavailability of heavy metals in polluted soils to rice, Commun. Soil Sci. Plant Anal. 41 (2010) 820–831.

[64] U. Roland, F. Holzer, U. Trommler, C. Hoyer, C. Rabe, M. Kraus, J. Schneider, F.D. Kopinke, Applications of radio-frequency heating in environmental technologies, Tech. Proc. Eng. 42 (2012) 161–164.

[65] E. Spain, A. Venkatanarayanan, Review of physical principles of sensing and types of sensing materials, Comput. Mater. Proc. 13 (2014) 5–46.

[66] J. Lee, H.S. Kim, H.Y. Jo, M.J. Kwon, Revisiting soil bacterial counting methods: Optimal soil storage and pretreatment methods and comparison of culture-dependent and -independent methods, PLoS ONE 10 (2021) e0246142.

[67] X. Tang, D.A. Cronin, N.P. Brunton, The effect of radio frequency heating on chemical, physical and sensory aspects of quality in turkey breast rolls, Food Chem. 93 (2005) 1–7.

[68] F. Marra, L. Zhang, J.G. Lyng, Radio frequency treatment of foods: Review of recent advances, IEEE J. Food Eng. 91 (2009) 497–508.

[69] S. Santalunai, C. Thongsopa, T. Thosdeekoraphat, The efficiency of dielectric heating by using symmetrically electric power ports on electrode plate for pest control, in: International Conference on Electrical Engineering/Electronics, Computer, Telecommunications and Information Technology, 2015, pp. 1–4.

[70] K. Ratniyomchai, S. Santalunai, T. Thosdeekoraphat, C. Thongsopa, Radio frequency treatment of foods: Review of recent advances, Appl. Mech. Mater. 343 (2013) 101–105.

[71] C. Srisuma, S. Santalunai, T. Thosdeekoraphat, C. Thongsopa, The analysis and design of milk pasteurization system by using radio frequency electric fields, in: Proceedings of the Asia-Pacific International Symposium on Electromagnetic Compatibility, 2017, pp. 158–160.

[72] C. Sutacha, S. Santalunai, C. Thongsopa, T. Thosdeekoraphat, W. Penkhrue, Inactivation of contaminated fungi in rice grains by dielectric heating, Appl. Sci. 12 (2022) 10478.

[73] W. Wasusathien, S. Santalunai, T. Thosdeekoraphat, C. Thongsopa, Rice types classification by using dielectric properties measurement with saline water increasing technique, in: Proceedings of the 9th International Symposium on Electrical Insulating Materials, 2020, pp. 433–438.

[74] S. Kornsing, S. Santalunai, T. Thosdeekoraphat, C. Thongsopa, Dielectric property measurement of freshwater fishes and parasite affecting infection opisthorchis viverrini for dielectric heating application, in: Proceedings of the 9th International Symposium on Electrical Insulating Materials, 2020, pp. 439–442.

[75] R.K. Douglas, S. Nawar, M.C. Alamar, F. Coulon, A.M. Mouazen, Almost 25 years of chromatographic and spectroscopic analytical method development for petroleum hydrocarbons analysis in soil and sediment: state-of-the-art, progress and trends, Environ. Sci. Technol. 47 (2017) 1497–1527.

[76] S. Lin, L. Gao, Y. Yang, J. Chen, S. Guo, M. Omran, G. Chen, Dielectric properties and high temperature thermochemical properties of the pyrolusite-pyrite mixture during reduction roasting, J. Mater. Res. Technol. 9 (2020) 13128–13136.

[77] A.H. Abdelgwad, T.M. Said, Design of ground penetrating radar antenna for detecting soil contamination at l-band frequencies, J. Microw. Opt. Technol. Lett. 16 (2017) 853–866.

[78] M.D. Ghazali, O. Zainon, K.M. Idris, S.N.A. Zainon, M.N.A. Karim, S.A. Anshah, N.F.A. Talib, The assessment of relative permittivity on diesel vapour in the moisture content of terap red soil by ground penetrating radar, Air Soil Water Res. 13 (2020) 1–11.

[79] A. Godio, Open ended-coaxial cable measurements of saturated sandy soils, Am. J. Environ. Sci. 3 (2007) 175–182.

[80] T. Yodrot, S. Santalunai, C. Thongsopa, T. Thosdeekoraphat, N. Santalunai, Measurement of dielectric properties in soil contaminated by biodiesel-diesel blends based on radio frequency heating, Appl. Sci. 13 (2023) 1248.

[81] V.V. Komarov, Handbook of Dielectric and Thermal Properties of Materials at Microwave Frequencies, Artech House, UK, 2012.